DOI: 10.13009/EUCASS2023-027
Aerospace Europe Conference 2023 – 10TH EUCASS – 9TH CEAS

6-DOF Orbit-attitude Stabilization around an Asteroid by using Performance-based Intermittent Event-triggered Control

Hongyi Xie[*†] *and Franco Bernelli-Zazzera*[*]
[*] *Department of Aerospace Science and Technology, Politecnico di Milano*
Via La Masa, 34 20156 Milano

hongyi.xie@polimi.it – franco.bernelli@polimi.it
[†] Corresponding Author

Abstract

This paper presents a barrier-based event-triggered orbital control scheme using intermittent controlled thrusts to confine a spacecraft within a narrow orbital radius around an asteroid. This ensures spacecraft safety and enables normal operation of on-board detection devices. The proposed method allows sufficient time gap between control impulses, enhancing the responsiveness of the global monitoring and decision system. Additionally, an adaptive attitude controller is designed to stabilize the spacecraft's orientation with respect to the Sun, contributing to orbital motion stability. Numerical simulations validate the reliable performance and robustness of the proposed control strategy.

1. Introduction

In recent years, there has been significant advancement in the number and scope of space missions focused on asteroids. These missions are driven by the desire to gain valuable insight into the formation of the solar system, as well as the potential risks associated with asteroid impacts and the abundant resources they hold. An essential phase in asteroid exploration is the probe closing phase before final landing or impact. One optimal approach during this phase is to stabilize the probe within the orbital stability zones surrounding the asteroid, such as those identified for asteroid 99942 Apophis [1], or to maintain probe hover in a fixed position or within a narrow area near the asteroid [2]. However, not all asteroids offer suitable orbital stability zones or hover points due to their irregular shape and uneven mass distribution. In previous asteroid missions like JAXA's Hayabusa-2 [3], to fully benefit from orbit-fixed location hovering, the probe had to remain approximately 20 km away from asteroid 25143 Itokawa for most of the time on a sun-synchronized orbit. It then rapidly decreased its orbital altitude to approach the asteroid for final landing, leaving limited time for certain mission objectives, such as creating a high-resolution global map of the asteroid [4]. In contrast, NASA's OSIRIS-Rex mission achieved long-term surrounding orbital operation by maintaining an orbit around asteroid 101955 Bennu at an altitude below 2 km for several months [5]. To accomplish this, NASA employed a complex combination of thrusters and dedicated numerous observation devices to monitor the probe's status, particularly after each utilization of the high-thrust main engines.

The OSIRIS-Rex mission experience highlighted the importance of maintaining the spacecraft's orbital altitude within a narrow error range for several days. This ensures the consistent functioning of fixed devices required for specific scientific missions, which will be even more crucial in future missions. For example, continuous monitoring of the inner structure variation of an impacted asteroid using Synthetic Aperture Radar (SAR), as an extension of the LICIACube's role in the DART mission [6]. It should be noted that OSIRIS-Rex is equipped with four high-thrust engines, six medium thrust engines, and a pair of low-thrust engines [5] for orbital motion. In the event of a failure or suspension of the low-thrust engines, like what occurred in the Hayabusa-1 probe [7], relying solely on thrust engines becomes necessary to maintain the spacecraft within the desired orbital altitude range for continuous normal operation of specialized space scientific tasks. While artificial commands can address this issue, the significant distance between an asteroid and Earth may result in delayed response to real-time state signals. Therefore, the implementation of an

DOI: 10.13009/EUCASS2023-027

autonomous guidance, navigation, and control system is preferable, with human engineers monitoring spacecraft states in a timely manner using various remote sensing methods. It would be particularly advantageous if the spacecraft's motion after each thrust event could be observed promptly through remote sensing techniques.

One effective method to confine the spacecraft within a narrow distance range from the asteroid is to establish both a minimum and maximum allowable distance from the asteroid's centre. When the spacecraft approaches the maximum allowable distance, a thrust is generated in the direction from the spacecraft towards the asteroid's centre to keep the spacecraft below the maximum orbital height threshold. Conversely, a thrust is applied in the opposite direction to raise the spacecraft's orbital height if it falls below the minimum allowance. However, careful design of the control thrust magnitude is necessary, considering the potential issue of actuator saturation, as the maximum control thrust may not always be sufficient to keep the spacecraft within the allowed barrier. A promising approach to restrict the probe's motion within a narrow orbital height area is to employ a barrier-function based event-triggered mechanism to determine when and where to generate the control thrust, as demonstrated in the pioneering work by Ong et al. [8]. The proposed control scheme successfully constrained the spacecraft around the asteroid during a 4-day simulation. However, several challenges still need to be addressed based on this research:

1. The complexity and physical significance of the triggered mechanism need further clarification. Additionally, the uneven distribution of time gaps between each triggered thrust remains a challenge. Although the latest preprint by the same author [9] appears to address this issue, a theoretical explanation is still lacking. A similar situation arose in spacecraft attitude control, where a high minimum inter-execution time was observed in numerical simulations [10] without corresponding theoretical explanation. However, this was subsequently addressed by a specially designed event-triggered mechanism based on the sigmoid function [11], which ensured the high minimum inter-execution time. Therefore, it would be beneficial to develop an event-triggered control scheme that guarantees a high minimum inter-event time in this scenario. This scheme should demonstrate its performance through numerical simulations and provide a theoretical analysis to explain its underlying logic. These challenges are expected to be tackled in future research.

2. The orbital dynamics function presented in [8] and [9] lacks completeness as it fails to consider the coupled motion between the self-spinning of the asteroid and the orbital motion of the spacecraft. Additionally, two significant perturbations were not considered. The first perturbation is the gravity gradient forces, which amount to approximately 1/30 of the polyhedron gravity as observed in the numerical simulations in this study. The second perturbation is the solar radiation pressure, which is particularly relevant when dealing with a celestial body with minimal gravitational forces, such as a small-sized asteroid. Both perturbations constitute non-negligible external forces that should be considered in future investigations.

3. The above-mentioned missing components in [8] and [9], namely the self-spinning of the asteroid, gravity gradient forces, and solar radiation pressure, are crucial factors contributing to orbit-attitude coupling in the orbital motion around an asteroid. The self-spinning of the asteroid becomes entangled with the orbital velocity and the vector of orbital radius in the orbital dynamics function. Similarly, the gravity gradient force gives rise to gravity gradient torques in the attitude dynamics function, while the solar radiation pressure introduces corresponding torques. Therefore, it is essential to consider the attitude motion when designing an orbital control system around an asteroid, accounting for the coupled motion resulting from the solar radiation pressure and gravity gradient [12].

Moreover, it has been demonstrated that orbit hovering around an asteroid can be achieved solely through attitude control [13], underscoring the significant role of attitude motion that cannot be neglected in near-asteroid orbital motion. Dynamics models for attitude-orbit coupled spacecraft in the vicinity of an asteroid have been established in [14] and [15], incorporating polyhedron gravitational models that account for gravity gradient and solar radiation pressure. Due to limitations in human technological capabilities, researchers often have access to rough estimates of an asteroid's mass and can only obtain its surface's figure with varying luminosity. To represent the asteroid's shape, the polyhedron method is commonly employed, assuming a homogeneous density distribution. Thus, the polyhedron method serves as a reliable approach to establishing the gravitational field of an asteroid [16].

Based on the orbit-attitude coupled dynamics system developed from the polyhedron gravitational model of the asteroid 25143 Itokawa, this paper proposes a novel event-triggered control strategy to maintain the spacecraft within a narrow safety distance range between the spacecraft and the centre of the asteroid by using only thrusters in orbit-attitude coupled control, just like the following picture depicts:

DOI: 10.13009/EUCASS2023-027

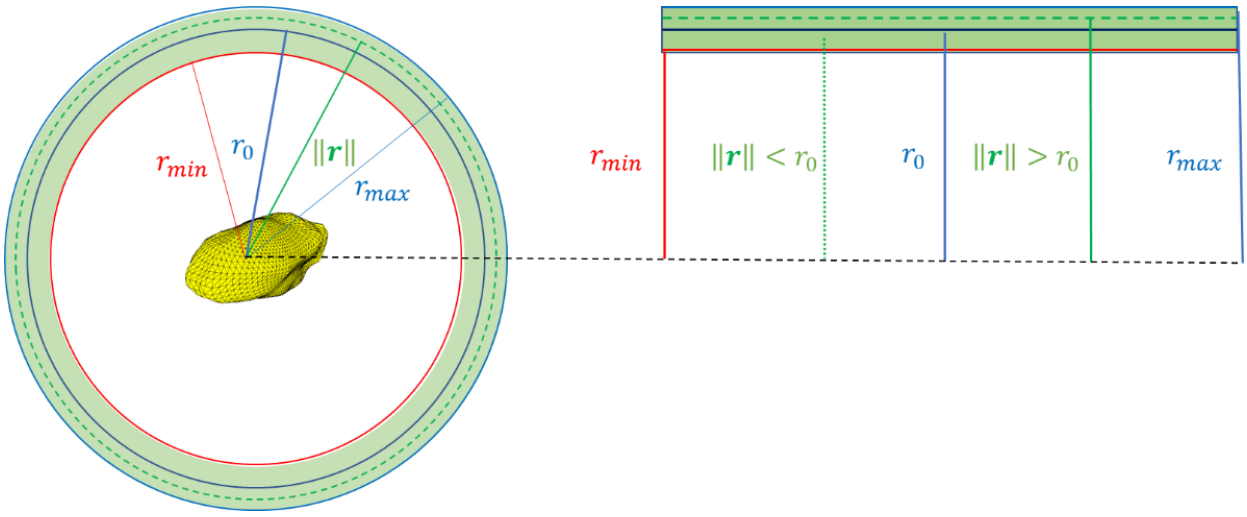

Fig. 1. The distribution of the allowed flying area with upper bound barrier and lower bound barrier

This event-triggered control system is quite different from all the previous control systems proposed in the field of aerospace engineering, because the event-triggered control system was always designed to cope with a problem called limited communication existing in the spacecraft with employment of wireless network to transmit signals in the control system, just like that proposed in [17] in which the control input is continuous but just change on the triggering instants. By contrast, the aim of event-triggered control in this paper is to ensure the system states within the safety range, and the control input is intermittent in orbit control in this paper. The orbital motion analysis takes a very vital part in the design of this event-triggered control scheme, and it can be extended to other cases about the orbit control and attitude control of spacecraft.

The remainder of this paper is organized as follows: Section 2 develops the orbit-attitude coupled dynamics model in the vicinity of an asteroid. Section 3 details the theoretical framework of the proposed event-triggered control schemes with the physical meaning of the barrier-based ETM. Section 4 presents the numerical simulation, highlighting the performance and robustness of the proposed control strategy. Finally, Section 5 summarizes the findings, discusses potential future research directions, and concludes the paper.

2. Orbit-attitude coupled dynamics model in the vicinity of an asteroid

In the dynamics system with a spacecraft in the vicinity of an asteroid, the orbit motion of the spacecraft and the implicit self-spinning of the asteroid is coupled as the following dynamics equation [18] depicts:

$$m\ddot{\mathbf{r}} + 2m(\boldsymbol{\Omega}_T \times \dot{\mathbf{r}}) + m\big(\boldsymbol{\Omega}_T \times (\boldsymbol{\Omega}_T \times \mathbf{r})\big) = m\mathbf{g}(\mathbf{r})_{pg} + \mathbf{f}(\mathbf{r}, \boldsymbol{\sigma})_{gg} + \mathbf{f}_{SRP} + \boldsymbol{\tau} \tag{1}$$

where m is the mass of the spacecraft, $\boldsymbol{\tau}$ is the control input, $\mathbf{r} = [\boldsymbol{x} \quad \boldsymbol{y} \quad \boldsymbol{z}]^{\boldsymbol{T}}$ is the position vector from the center of mass of the asteroid to the center of mass of the spacecraft in the asteroid body frame, and $\boldsymbol{\Omega}_T = [0 \quad 0 \quad \omega_T]^{\boldsymbol{T}}$ is the constant angular velocity vector that depicts the self-spinning of the asteroid. According to JAXA's exploration [19] , the self-spin period of the asteroid 25143 Itokawa is equal to 12.132 hours [20], and thus there exists $\omega_T = 0.003596 deg/s$.

Besides, $\mathbf{g}(\mathbf{r})_{pg}$ denotes the force due to the polyhedral gravity model of the asteroid. For an asteroid which is in accordance with the assumption of homogeneity, a rational way to get the polyhedral gravity is to decompose the surface of an asteroid into several triangular facets approximately with shared edge sides, and therefore an asteroid can be seen as a composition of several interconnected triangular pyramid [21], which is shown by Fig. 2 as follows:

DOI: 10.13009/EUCASS2023-027

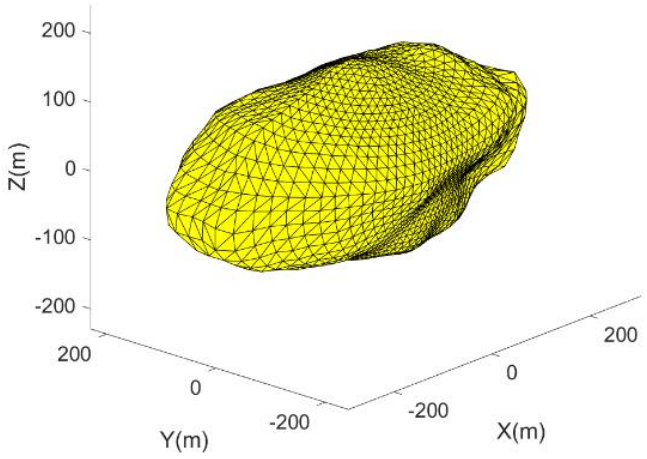

Fig. 2. A visual polyhedral model of the asteroid 25143 Itokawa with 3688 triangular facets, 1846 triangular vertical points and 5532 triangular edge sides.

Thus, the gravitational forces exerted on a spacecraft in the vicinity of an asteroid is equal to the composition of the gravitational forces generated by each triangular pyramid. To determine the positions and directions of every different edge, and to regulate the shapes of every different triangle, it's necessary to define a series of vectors as follows [22-23]:

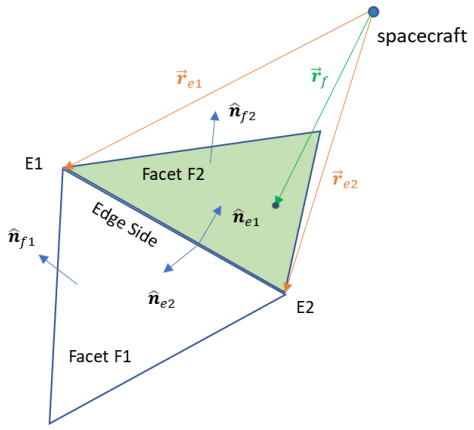

Fig. 3. The relative relationships of facets and edges in the polyhedron model

As Fig. 2 demonstrates, each part of the surface of the asteroid can be seen as two triangular facets $F1$, $F2$ with one shared edge side $E1E2$ and two shared vertices $E1$ and $E2$. The following unit vectors are defined to illustrate the positions and directions of all the facets in the asteroid mass center centered 3-axes coordinated label system: $\hat{\boldsymbol{n}}_{f1} \perp F1$ and $\hat{\boldsymbol{n}}_{f2} \perp F2$ are two plane normal unit vectors to illustrate the direction of two near facets. Furthermore, $\hat{\boldsymbol{n}}_{e1} \perp E1E2$ with $\hat{\boldsymbol{n}}_{e1} \parallel F1$ and $\hat{\boldsymbol{n}}_{e2} \perp VP1VP2$ with $\hat{\boldsymbol{n}}_{e2} \parallel F2$ are two edge side normal unit vectors to decide the position and direction of the edge side $VP1VP2$. Then the following constants are designed to symbolize the different edge sides and facets:

$$\boldsymbol{N}_e = \hat{\boldsymbol{n}}_{f1}\hat{\boldsymbol{n}}_{e1} + \hat{\boldsymbol{n}}_{f2}\hat{\boldsymbol{n}}_{e2} \tag{2}$$

$$\boldsymbol{N}_f = \hat{\boldsymbol{n}}_f\hat{\boldsymbol{n}}_f^T \tag{3}$$

Moreover, the vector pointed from the spacecraft to a point on a facet is defined as $\boldsymbol{r}_f$, and then the vector pointed from the spacecraft to the 2 vertical points on the different sides of an edge side is given as $\boldsymbol{r}_{e1}, \boldsymbol{r}_{e2}$, then the potential owing to the edge side can be acquired as follows:

DOI: 10.13009/EUCASS2023-027

$$P_e = \ln(\|\boldsymbol{r}_{e1}\| + \|\boldsymbol{r}_{e2}\| + \|\boldsymbol{r}_e\|) - \ln(\|\boldsymbol{r}_{e1}\| + \|\boldsymbol{r}_{e2}\| - \|\boldsymbol{r}_e\|) \tag{4}$$

where $\boldsymbol{r}_e$ is equal to the vector $\overrightarrow{E1E2}$ in Fig. 2, Define the 3 different unit vectors $\hat{\boldsymbol{r}}_{f1}, \hat{\boldsymbol{r}}_{f2}, \hat{\boldsymbol{r}}_{f3}$ from the spacecraft to the 3 vertical points of a triangular facet leads to a factor to symbolize different facet as follows:

$$\omega_f = 2\arctan\left[\hat{\boldsymbol{r}}_{f1} \cdot \hat{\boldsymbol{r}}_{f2} \times \hat{\boldsymbol{r}}_{f3} / \left(1 + \hat{\boldsymbol{r}}_{f1} \cdot \hat{\boldsymbol{r}}_{f2} + \hat{\boldsymbol{r}}_{f2} \cdot \hat{\boldsymbol{r}}_{f3} + \hat{\boldsymbol{r}}_{f3} \cdot \hat{\boldsymbol{r}}_{f1}\right)\right] \tag{5}$$

Then it's reasonable to get the term $\mathbf{g}(\mathbf{r})_{pg}$ that represents the gravitational acceleration due to the asteroid under the premise of polyhedron hypothesis as follows:

$$\mathbf{g}(\boldsymbol{r})_{pg} = \rho G \left(\sum_{edge\ sides} P_e \boldsymbol{N}_e \boldsymbol{r}_e - \sum_{facets} \omega_f \boldsymbol{N}_f \boldsymbol{r}_f \right) \tag{6}$$

where $\rho = 1950\ kg/m^3$ is the average density of asteroid 25143 Itokawa in this case [24] and $G = 6.6743 \times 10^{-11} m^3 \cdot kg^{-1} \cdot s^{-2}$ is the gravitational constant.

Except for $\mathbf{g}(\boldsymbol{r})_{pg}$, the term $\mathbf{f}(\mathbf{r}, \boldsymbol{\sigma})_{gg}$represents the gravitational gradient force arising from the interaction between point mass gravity model of the asteroid and the rigid body model of the spacecraft. According to [22-23], the term $\mathbf{f}(\mathbf{r}, \boldsymbol{\sigma})_{gg}$ is given as follows:

$$\mathbf{f}(\mathbf{r}, \boldsymbol{\sigma})_{gg} = -3GM[\boldsymbol{J} + tr(\boldsymbol{J})/2 - 5(\hat{\boldsymbol{r}}^{\boldsymbol{T}} \boldsymbol{J} \boldsymbol{r}) \boldsymbol{I}_{3\times3}]\, \boldsymbol{r}/\|\boldsymbol{r}\|^5 \tag{7}$$

where $M = 3.58 \times 10^{10} kg$ is the mass of the asteroid 25143 Itokawa [22-23], $\boldsymbol{J}$ denotes the inertia matrix of the spacecraft, $\mathrm{tr}(\boldsymbol{J})$ is the trace of $\boldsymbol{J}$, and $\boldsymbol{I}_{3\times3}$ represents an identity matrix. Besides, the SRP force under an ideal hypothesis model of flat model with continuous maximizing power output is presented as follows [12] :

$$\mathbf{f}_{SRP} = -\left[2(C_s + C_d/3)\hat{\boldsymbol{n}}_{fp} + (C_d + C_a)\hat{\boldsymbol{n}}_{sp}\right] PA \tag{8}$$

where C_s, C_d, C_a are design parameters regarding the optical characters of the spacecraft, $\hat{\boldsymbol{n}}_{fp}$ denotes the normal unit vector which is orthogonal to the solar panel plane of the spacecraft, and $\hat{\boldsymbol{n}}_{sp}$ denotes the normal unit vector directed from the spacecraft to the Sun. Besides, $P = P_0/d_s^2$, where $P_0 = 1 \times 10^{17} kg \cdot m \cdot s^{-2}$ is a constant regarding the SRP, and d_s denotes the distance from the Sun to the spacecraft. To maximize the energy absorption from the sun, the aim of attitude control in this paper is to align $\hat{\boldsymbol{n}}_{fp}$ with $\hat{\boldsymbol{n}}_{sp}$, and the corresponding attitude dynamics model is demonstrated as follows:

$$\boldsymbol{J}\dot{\boldsymbol{\omega}} = -\boldsymbol{\omega}^{\times} \boldsymbol{J} \boldsymbol{\omega} + \boldsymbol{T}_{SRP} + \boldsymbol{T}_{gg} + \boldsymbol{u} \tag{9}$$

where $\boldsymbol{\omega}$ denotes the angular velocity of the spacecraft under its own body label coordinate system, $\boldsymbol{u}$ denotes the control torques, and the SRP-induced torque $\boldsymbol{T}_{SRP}$ is shown as follows:

$$\boldsymbol{T}_{SRP} = \boldsymbol{L}_{\boldsymbol{SRP}} \times m\boldsymbol{a}_{SRP} = [0 \quad L \quad 0]^T \times \mathbf{f}_{SRP} \tag{10}$$

where L represents the distance between the spacecraft's mass center and the forced center of $\mathbf{f}_{SRP}$. Besides, it's reasonable to demonstrate the gravity gradient torque $\boldsymbol{T}_{gg}$ as follows [22-23]:

$$\boldsymbol{T}_{gg} = 3GM\boldsymbol{r}^{\times} \boldsymbol{J} \boldsymbol{r}/\|\boldsymbol{r}\|^5 \tag{11}$$

Besides, the attitude kinematics model written in the form of quaternion is presented as follows:

$$\dot{\boldsymbol{q}}_v = (\boldsymbol{q}_v^{\times} + q_0 \boldsymbol{I}_{3\times3})\, \boldsymbol{\omega}/2\,, \dot{q}_0 = -\boldsymbol{q}_v^T\, \boldsymbol{\omega}/2 \tag{12}$$

where $\boldsymbol{q}_v = [q_1 \quad q_2 \quad q_3]^T$ is the vector part of attitude quaternion and q_0 is the corresponding scalar part. Furthermore, $\mathbf{f}_{SRP}$ can be rewritten as

$$\mathbf{f}_{SRP} = 2(C_s + C_d/3) PA \boldsymbol{q}_{\boldsymbol{v}}^T \tag{13}$$

DOI: 10.13009/EUCASS2023-027

Equations $(1)-(12)$ illustrate the dynamics model of a spacecraft in the vicinity of an asteroid. It's observed from equation (10) that the term $\mathbf{f}_{SRP}$ appears in both the orbit dynamics function (1) and the attitude dynamics function (9). Furthermore, there exists the following equation:

$$\boldsymbol{T}_{gg} = 3GM\boldsymbol{r}^{\times}\boldsymbol{J}\boldsymbol{r}/\|\boldsymbol{r}\|^5 = -\boldsymbol{r}^{\times}\boldsymbol{J}\mathbf{f}(\mathbf{r},\boldsymbol{\sigma})_{gg}[\boldsymbol{J} + tr(\boldsymbol{J})/2 - 5(\hat{\boldsymbol{r}}^{\boldsymbol{T}}\boldsymbol{J}\boldsymbol{r})\boldsymbol{I}_{3\times3}]^{-1} \tag{14}$$

which implies that there exists orbit-attitude coupling owing to both the SRP and the gravity gradient. Based on the orbit-attitude coupled dynamics model illustrated in $(1-12)$, a barrier-based event-triggered control scheme is proposed to realize the aim of orbit stabilization with the assistance of attitude stabilization for coupled motions, which is illustrated in the following section.

3. Barrier-based Event-triggered Control Systems

The control system design can be divided into two distinct parts: orbital control and attitude control. Orbital control takes on the primary role and utilizes a barrier-based event-triggered mechanism to determine the optimal timing and location for initiating orbital thruster propulsion. On the other hand, attitude control serves as a supporting component, addressing the challenges of orbital instability resulting from orbit-attitude coupling in orbital control. Additionally, the attitude control system ensures Sun-synchronization, which is crucial for the mission's requirements.

3.1 Orbital Control Systems

Confining a spacecraft within a restricted range of distance to the center of the asteroid means the spacecraft must move within a spherical shell, which is upper bounded by a large sphere barrier with its radius r_{max}, and lower bounded by a small sphere barrier with its radius r_{max}, just like that demonstrated by Fig. 1. Define $r_0 = (r_{max} + r_{min})/2$, which is an ideal distance from the spacecraft to the center of the asteroid but hard to maintain by using only thrusters. However, $\|\boldsymbol{r}\| = r_0$ is a good line of demarcation to separate the allowed flying area. It's viable to design a subtle event-triggered mechanism by utilizing the properties just opposite beyond and below the orbital radius $r_0 = (r_{max} + r_{min})/2$, which is discussed as follows:

Case 1: For the spacecraft orbiting within the upper area bounded by $r_0 \le \|\boldsymbol{r}\| < r_{max}$, there exists the following two situations:

1. $d\|\boldsymbol{r}\|/dt \le 0$, which implies that the altitude of the spacecraft is decreasing. Consider that the spacecraft can only escape from the upper area with $d\|\boldsymbol{r}\|/dt > 0$, no control thrust is needed in this situation.

2. $d\|\boldsymbol{r}\|/dt > 0$, while the expected highest orbital altitude is no higher than the upper limit of the barrier area. Consider that the gravity of asteroid plays a dominant role in the combined external forces that the spacecraft suffers, there must exist $d^2\|\boldsymbol{r}\|/dt^2 < 0$. Thus, no control thrust is needed in this situation.

3. $d\|\boldsymbol{r}\|/dt > 0$, while the expected highest orbital altitude may be higher than the upper limit of the barrier area. In this case the spacecraft may break through the upper limit of the allowed flying area, and the control thrust must be executed before the off-line occurs.

Case 2: For the spacecraft orbiting within the lower area bounded by $r_{min} \le \|\boldsymbol{r}\| < r_0$, there exists the following two situations:

1. $d\|\boldsymbol{r}\|/dt \ge 0$, which implies that the altitude of the spacecraft is increasing. Consider that the spacecraft can only escape from the lower area with $d\|\boldsymbol{r}\|/dt < 0$, no control thrust is needed in this situation.

2. $d\|\boldsymbol{r}\|/dt < 0$. Considering that the gravity of asteroid plays a dominant role in the combined external forces that the spacecraft suffers, the spacecraft is bound to lose its altitude without necessary lift forces.

According to the discussion, the same tendency of some vectors implies just the opposite tendency of off-line risk. Besides, the orbital radius vector $\boldsymbol{r}$ alone or solo the orbital velocity vector $\boldsymbol{v}$ alone will not be a good choice of entire event-triggered mechanism, while their product is a good candidate for the event-triggered mechanism. The product $\boldsymbol{rv}$ demonstrates just the opposite situation beyond and below the mid orbital radius. For the above case 1, $\boldsymbol{rv} > 0$ implies that the spacecraft is rising, and higher $\boldsymbol{rv} > 0$ means a stronger tendency that the spacecraft will rise to escape from the upper limit. By contrast, $\boldsymbol{rv} < 0$ means the spacecraft is falling and there will be no risk of touching the

DOI: 10.13009/EUCASS2023-027

upper limit in case 1. However, for the above case 2, $\boldsymbol{rv} > 0$ and $\boldsymbol{rv} < 0$ will bring the signals with just the opposite meaning about the risk of off-line. All the analysis in this paragraph can be easily recognized by reading the following Fig. 4:

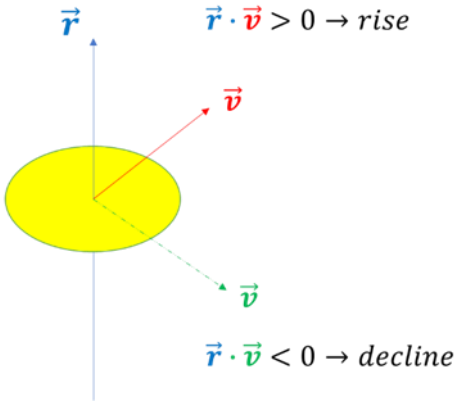

Fig. 4. The relationship between the orbital radius vector $\boldsymbol{r}$ and the orbital velocity vector $\boldsymbol{v}$

Thus, an additional term that just opposite beyond and below $\|\boldsymbol{r}\| = r_0$ is enough to ensure that the event-triggered mechanism is the same one beyond and below $\|\boldsymbol{r}\| = r_0$, and the event-triggered mechanism is designed as follows:

$$t_k = \min\left\{\frac{r_0 - \|\boldsymbol{r}\|}{\|\boldsymbol{r}\|}\boldsymbol{rv} + \alpha \leq 0\right\}, k = 1,2,\ldots \tag{15}$$

where $\alpha > 0$ is a design parameter, and the orbital range of the spacecraft can be restricted just by tuning the parameter α. Once the inequation (15) is violated the thrusters will be activated to generate propulsion forces to drive the spacecraft back to the opposite direction along the direction of orbital radius to ensure the safety of the spacecraft. Furthermore, it's reasonable to propose an impulsive orbital control scheme as follows:

$$\boldsymbol{\tau} = K_1 sgn(r_0 - \|\boldsymbol{r}\|)(r_0 - \|\boldsymbol{r}\|)\frac{\boldsymbol{r}}{\|\boldsymbol{r}\|} tanh\left(\frac{r_0 - \|\boldsymbol{r}\|}{r_0 - r_{min}}\right) \tag{16}$$

where $K_1 > 0$ is the control gain. If $\|\boldsymbol{\tau}\| \geq F_M$, then the controlled thrusts should follow:

$$\boldsymbol{\tau} = F_M sgn(r_0 - \|\boldsymbol{r}\|)\frac{\boldsymbol{r}}{\|\boldsymbol{r}\|} \tag{17}$$

where $F_M > 0$ is the maximum output thrust that the thrusters can generate, and the working time length of the thrusters is set as a short, fixed time length just after the triggering instant. It's not difficult to promise that such a control system can keep the spacecraft away from the upper barrier with the help of an event-triggered mechanism (15) designed properly, which can be verified by corresponding numerical simulation.

3.2 Attitude Control System

The aim of the attitude control system is to ensure attitude stabilization, to further avoid the negative influence in orbital motion owing to orbit-attitude coupling. Based on the sliding vector $\boldsymbol{s} = \boldsymbol{\omega} + k_1\boldsymbol{q}_v$ with $k_1 > 0$, the attitude controller is proposed as follows:

$$\boldsymbol{u} = -K_2\boldsymbol{s} - \hat{b}Tanh\,(\rho\boldsymbol{s}) \tag{18}$$

where $K_2 > 0$ is the control gain, $\rho > 0$ is a design parameter, $Tanh\,(\rho\boldsymbol{s}) = [tanh(\rho s_2) \quad tanh(\rho s_2) \quad tanh(\rho s_3)]^T$, and $\hat{b} > 0$ is an adaptive term varying with the following equation:

$$\dot{\hat{b}} = c\|\boldsymbol{s}\| - c_1\hat{b} \tag{19}$$

DOI: 10.13009/EUCASS2023-027

where $c, c_1, \hat{b}(0) \geq 0$ are design parameters. The performance and robustness of the proposed attitude control system can be observed from the part of numerical simulation.

4.Numerical Simulation

In this section, a series of numerical simulations are carried out to demonstrate the brilliant performance of the designed control system. Consider of the characteristics of orbit-attitude coupled motion around an asteroid, a short step size equal to 0.25s is adopted in the numerical simulation to permit the normal running of the attitude dynamics and control system, while a relative long-time length of simulation equals to 12000s (200 min) is employed to make sure the spacecraft can surround the asteroid with an intact circle. Correspondingly, the expected orbital radius r_0 is set as only $200m$ to shorten the orbital period of the spacecraft, which means the perturbations from the asteroid and the coupling effects are magnified significantly compared to the case in a higher orbit, because the radius of the asteroid is close to 150m in corresponding orbital plane. Consider of this dangerous environment of task, the allowable error of orbital radius is set as only $\pm 5m$, the orbital radius of the spacecraft is restricted within the range $\|\boldsymbol{r}\| \in [195,205]$. Here, a reasonable hypothesis of the mission scenario is that the spacecraft takes detection devices to detect the layer with its orbital radius equal to 80m, the detection mission requires such a working orbital radius so that the devices can send detection wave and get relative return echo effectively.

For the simplicity, the initial orbital velocity of the spacecraft is selected as

$$v_0 = \begin{bmatrix} 0 & 0 & \sqrt{\dfrac{GM}{r_0}} \end{bmatrix}^T \tag{20}$$

where $G = 6.67 \times 10^{-11} N \cdot m^2 \cdot kg^{-2}, M = 3.58 \times 10^{10} kg$ [24]. The mass of the spacecraft is set as $m = 600kg$, and this spacecraft is assumed as a full-actuated spacecraft with thrust supplied in all the 3 directions of the axes of its own body coordinated label system. The maximum thrust in a single direction is set as 22N, which is equal to that of the orbital control thrusters fixed in NASA's OSIRIS-Rex. The orbital control gain is selected as $K_1 = 4$, the design parameter α in the event-triggered mechanism is set as $\alpha = 0.05$. Furthermore, the orbital control thrusters are assumed to work for 50s after each time of triggering. Besides, the inertial matrix of the spacecraft is assumed as

$$\boldsymbol{J} = \begin{bmatrix} 360 & 0 & 0 \\ 0 & 480 & 0 \\ 0 & 0 & 480 \end{bmatrix} kg \cdot m^2 \tag{21}$$

For the part of attitude dynamics and control, the initial attitude error is assumed as $[20 \quad -10 \quad 0]^T deg$, the initial angular velocity is set as $[0 \quad 0 \quad 0]^T deg/s$. The attitude control gain is set as $K_2 = 21$, with the selected parameter in sliding-mode term $k_1 = 0.08$. The adaptive parameters are chosen as $c = 143, c_1 = 2.3 \times 10^{-6}, \rho = 22$. Moreover, the area of the solar panel is set as $40m^2$. The light parameters C_s, C_d, C_a are set as $C_s = 0.1, C_d = 0.1, C_a = 0.4$, respectively. The distance from the asteroid to the sun is simplified to be 1AU, and the center divergence for inducing the SRP torque is set as 0.05m.

According to the selected parameters, the trajectory of the spacecraft can be obtained as follows:

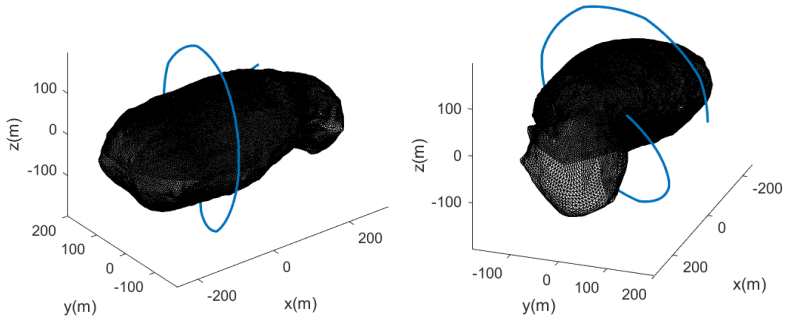

Fig.5 Orbit Trajectory around the asteroid

DOI: 10.13009/EUCASS2023-027

Fig. 5. depicts the trajectory of the spacecraft. It can be observed that the position of the spacecraft varies a lot on the direction of x-axis, which is shown much clearer by the following Fig. 6. To describe the spacecraft's position variation in 3-axes:

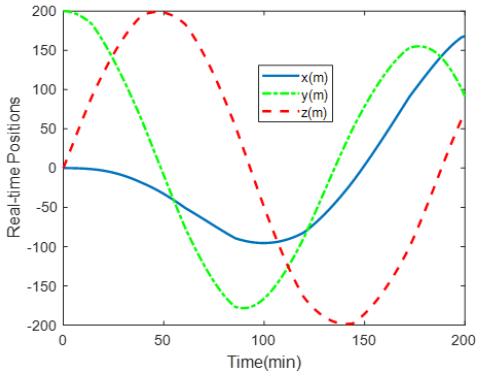

Fig.6 The projection of the position of the spacecraft on 3-axes

Thus, the projection of the trajectory on y-z plane cannot be a constructive figure in this paper. Instead, a direct description of the orbital radius can reveal the effect of the designed barrier-based orbital control system straightforwardly, which is shown as follows:

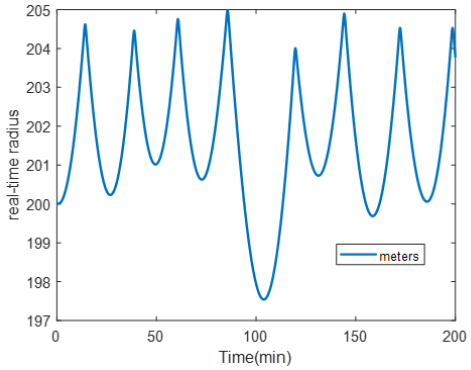

Fig.7 Orbital Radius

Fig. 7 illustrates the variation of the orbital radius. The orbital radius is constrained within the range $\|\boldsymbol{r}\| \in [195,205]$ successfully. According to the corresponding numerical experiment based on the same code, if the event-triggered parameter α is set as a value small enough, then the range of $\|\boldsymbol{r}\|$ can be constrained within a range of error within 0.01m, which reveals the strong ability of the designed event-triggered control scheme in high-precision orbital station keeping by using impulsive controlled propulsion. Besides, the orbital velocity of the spacecraft on 3 different axes is demonstrated in Fig. 8. as follows:

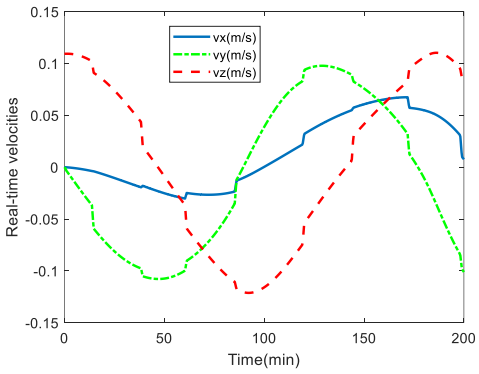

Fig.8 The projections of orbital velocity on 3-axes

DOI: 10.13009/EUCASS2023-027

Fig. 8. demonstrates the abrupt variation of orbital velocity clearly, while the variation is caused by the control thrusts exhibits as follows:

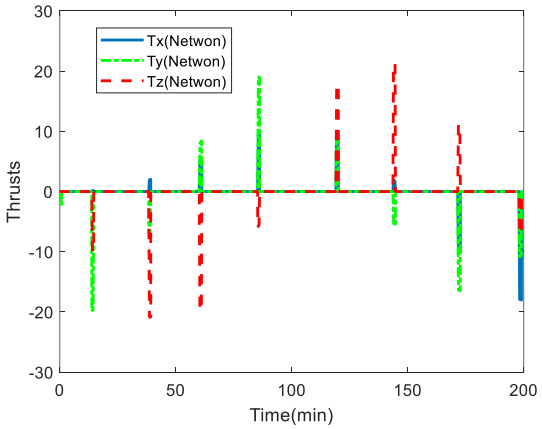

Fig.9 The control thrusts on 3 axes

It's observed that the control thrusts are impulsive, with their initial time of propulsion decided by the event-triggered mechanism.

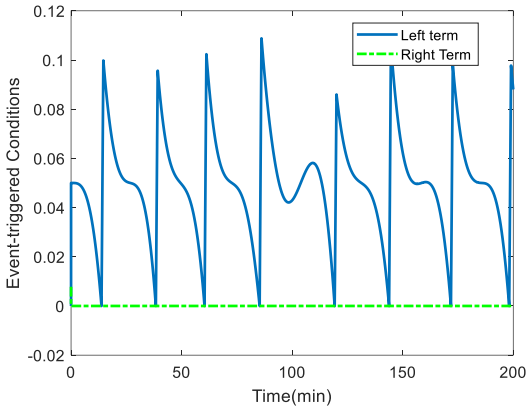

Fig.10 Event-triggering conditions

Fig. 10. illustrates the variation of the triggering condition. Once the inequation $\frac{r_0-\|\boldsymbol{r}\|}{\|\boldsymbol{r}\|}\boldsymbol{rv}+\alpha \leq 0$ is met, the thrusters will start to generate propulsion to bring the value of $\frac{r_0-\|\boldsymbol{r}\|}{\|\boldsymbol{r}\|}\boldsymbol{rv}+\alpha$ into a high number. The value of $\frac{r_0-\|\boldsymbol{r}\|}{\|\boldsymbol{r}\|}\boldsymbol{rv}+\alpha$ will decrease slowly relatively in the subsequent time, until it decreases to 0 to trigger the same event-triggered condition another time. Furthermore, Fig. 11 shows the distribution of the inter-execution time as follows:

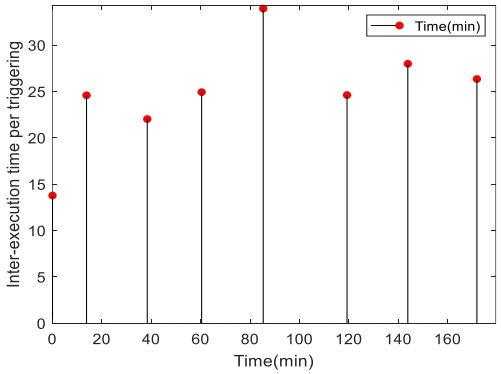

Fig.11 Inter-execution time

DOI: 10.13009/EUCASS2023-027

It’s observed that the event-triggered mechanism was triggered 8 times in 200 min, which leaves enough time for the ground station to transmit signals sent in the form of light. Besides, the effects of attitude stabilization are shown by Fig. 12-Fig.15. as follows:

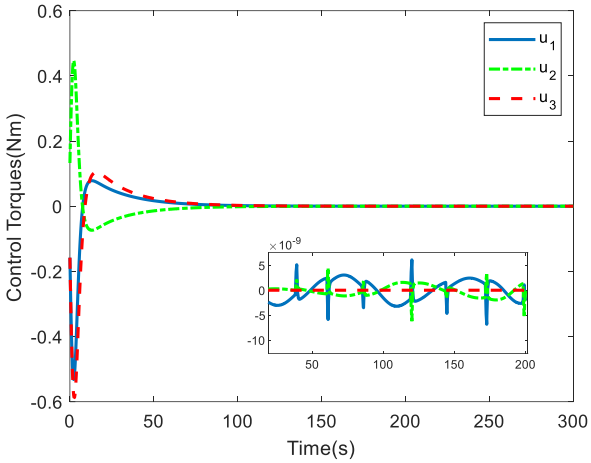

Fig.12 Attitude Control Torques

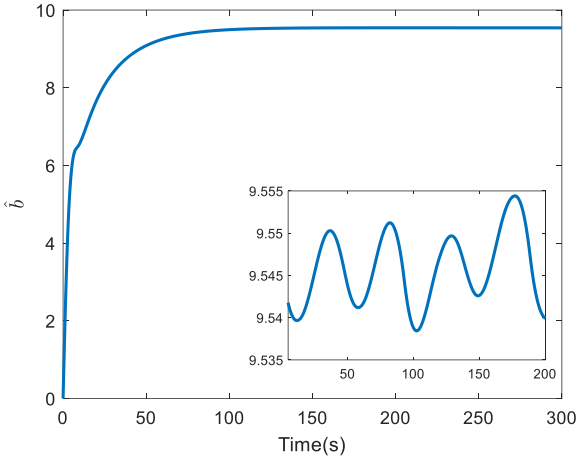

Fig.13 Adaptive parameter

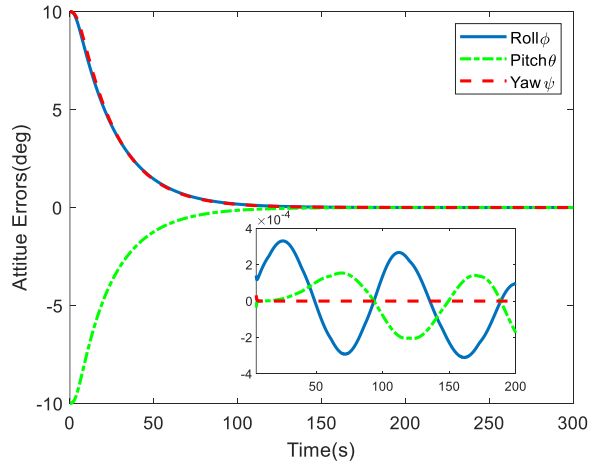

Fig.14 Attitude errors depicted in Euler angles

DOI: 10.13009/EUCASS2023-027

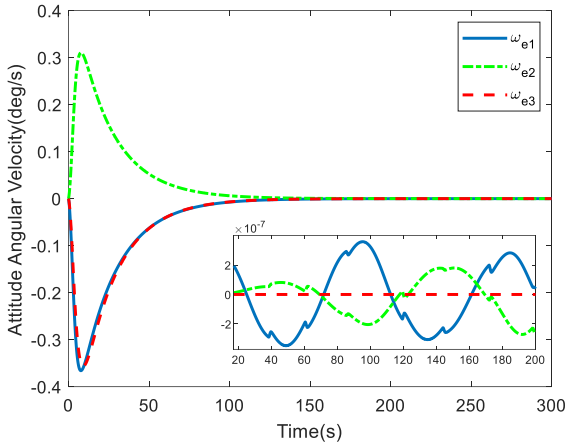

Fig.15 Attitude angular velocity

Note that the unit of time is second in the main figures of Fig. 12-Fig. 15. Nevertheless, small sub-figures inside the main figures are employed to depict the results of long-term evolution of the system states, and the time unit of these small subfigures are not seconds but minutes. According to Fig. 12-Fig. 15., the attitude angular velocity and the attitude errors shown in Euler Angles can converge within a small area around 0. Besides, the influence of orbital control and orbit-attitude coupling can be observed on Fig. 12. and Fig. 15. with obvious abrupt variations around the triggering instants, which shows the necessity of employing attitude control in barrier-based event-triggered impulsive thrusted control around an asteroid.

Conclusions

This paper presents a novel barrier-function-based event-triggered control scheme for effectively constraining the motion of a spacecraft within a narrow range of orbital radius around an asteroid. It’s very direct for any reader to recognize the physical meaning of the designed barrier-based event-triggered mechanism, which establish an easy and reliable barrier for restricting the spacecraft within an area with safety and special requirement of some on-board scientific devices.

The proposed approach addresses the challenges associated with motion variation and the control of attitude in 6-DOF orbit-attitude-coupled systems. Through simulation setup and experimental results, the performance and robustness of the proposed control strategy have been demonstrated. The findings indicate that the proposed approach outperforms existing methods, providing enhanced efficiency in maintaining the spacecraft within the desired orbital radius range. The control scheme's ability to optimize the time gaps between thrusts reduces the burden on the remote-sensing system, enabling timely monitoring and evaluation of the spacecraft's states.

This research contributes to the field of asteroid exploration by offering a comprehensive solution for orbit-attitude control that considers the specific challenges posed by irregularly shaped asteroids, gravitational gradient torques, solar radiation pressure and corresponding torques from the perspective of mission scenario, and intermittent working thrusters with actuator saturation owing to the spacecraft itself. The proposed approach has broader implications for orbital control and attitude control of spacecraft, highlighting the significance of considering both orbital and attitude dynamics in mission planning and design.

In summary, the barrier-function-based event-triggered control scheme presented in this paper offers a promising and effective strategy for maintaining spacecraft within a narrow orbital height range around asteroids by using only intermittent working thrusters. Further research and development in this area can lead to advancements in considering continuous low-thrust propulsion with vectored thrust. Otherwise, consider the underactuated spacecraft with intermittent thrusters in only 1 axis or 2 axes of orbit control, with attitude control to tune its direction before execute control thrusts under the orbit-attitude coupled dynamics system.

DOI: 10.13009/EUCASS2023-027

References

[1] Lang, A., 2021. Spacecraft orbital stability zones around asteroid 99942 Apophis. *Acta Astronautica*, *182*: 251-263.

[2] Zeng, X., Gong, S., Li, J. and Alfriend, K.T., 2016. Solar sail body-fixed hovering over elongated asteroids. *Journal of Guidance, Control, and Dynamics*, *39*(6): 1223-1231.

[3] Tsuda, Y., Yoshikawa, M., Abe, M., Minamino, H. and Nakazawa, S., 2013. System design of the Hayabusa 2—Asteroid sample return mission to 1999 JU3. *Acta Astronautica*, *91*: 356-362.

[4] Bennett, C.A., DellaGiustina, D.N., Becker, K.J., Becker, T.L., Edmundson, K.L., Golish, D.R., Bennett, R.J., Burke, K.N., Cue, C.N.U., Clark, B.E. and Contreras, J., 2021. A high-resolution global basemap of (101955) Bennu. *Icarus*, *357*: 113690.

[5] Lauretta, D.S., Balram-Knutson, S.S., Beshore, E., Boynton, W.V., Drouet d'Aubigny, C., DellaGiustina, D.N., Enos, H.L., Golish, D.R., Hergenrother, C.W., Howell, E.S. and Bennett, C.A., 2017. OSIRIS-REx: sample return from asteroid (101955) Bennu. *Space Science Reviews*, *212*: 925-984.

[6] Dotto, E., Della Corte, V., Amoroso, M., Bertini, I., Brucato, J.R., Capannolo, A., Cotugno, B., Cremonese, G., Di Tana, V., Gai, I. and Ieva, S., 2021. LICIACube-the Light Italian Cubesat for Imaging of Asteroids in support of the NASA DART mission towards asteroid (65803) Didymos. *Planetary and Space Science*, *199*: 105185.

[7] Yairi, T., Kawahara, Y., Fujimaki, R., Sato, Y. and Machida, K., 2006, July. Telemetry-mining: a machine learning approach to anomaly detection and fault diagnosis for space systems. In *2nd IEEE International Conference on Space Mission Challenges for Information Technology (SMC-IT'06)*, IEEE.

[8] Ong, P., Bahati, G. and Ames, A.D., 2022, December. Stability and safety through event-triggered intermittent control with application to spacecraft orbit stabilization. In *2022 IEEE 61st Conference on Decision and Control (CDC)*, 453-460. IEEE.

[9] Ong, P. and Ames, A.D., 2023. Intermittent Safety Filters for Event-Triggered Safety Maneuvers with Application to Satellite Orbit Transfers. *arXiv preprint arXiv:2304.08684*.

[10] Xie, H., Wu, B. and Liu, W., 2021. Adaptive neural network model-based event-triggered attitude tracking control for spacecraft. International Journal of Control, Automation and Systems, 19(1) : 172-185.

[11] Xie, H., Wu, B. and Bernelli-Zazzera, F., 2022. High minimum inter-execution time sigmoid event-triggered control for spacecraft attitude tracking with actuator saturation. IEEE Transactions on Automation Science and Engineering. 20(2) : 1349-1363.

[12] Kikuchi, S., Howell, K.C., Tsuda, Y. and Kawaguchi, J.I., 2017. Orbit-attitude coupled motion around small bodies: Sun-synchronous orbits with Sun-tracking attitude motion. *Acta Astronautica, 140*: 34-48.

[13] Petersen, C., 2016. *Advances in underactuated spacecraft control* (Doctoral dissertation).

[14] Shi, Y., Wang, Y. and Xu, S., 2017. Mutual gravitational potential, force, and torque of a homogeneous polyhedron and an extended body: an application to binary asteroids. *Celestial Mechanics and Dynamical Astronomy*, *129*: 307-320.

[15] Bolatti, D.A. and de Ruiter, A.H., 2020. Quantification of attitude effects on orbital dynamics near asteroids. *Acta Astronautica, 167* : 467-482.

[16] Werner, R.A., 1994. The gravitational potential of a homogeneous polyhedron or don't cut corners. *Celestial Mechanics and Dynamical Astronomy*, *59*: 253-278.

[17] Wu, B., Shen, Q. and Cao, X., 2018. Event-triggered attitude control of spacecraft. *Advances in Space Research*, *61*(3): 927-934.

[18] Scheeres, D.J., 2012. Orbital mechanics about small bodies. *Acta Astronautica*, *72*: 1-14.

[19] Demura, H., Kobayashi, S., Nemoto, E., Matsumoto, N., Furuya, M., Yukishita, A., Muranaka, N., Morita, H., Shirakawa, K., Maruya, M. and Ohyama, H., 2006. Pole and global shape of 25143 Itokawa. *Science*, *312*(5778): 1347-1349.

[20] Kaasalainen, M., Kwiatkowski, T., Abe, M., Piironen, J., Nakamura, T., Ohba, Y., Dermawan, B., Farnham, T., Colas, F., Lowry, S. and Weissman, P., 2003. CCD photometry and model of MUSES-C target (25143) 1998 SF36. *Astronomy & Astrophysics*, *405*(3): L29-L32.

[21] Werner, R. A., & Scheeres, D. J.,1996. Exterior gravitation of a polyhedron derived and compared with harmonic and mascon gravitation representations of asteroid 4769 Castalia. *Celestial Mechanics and Dynamical Astronomy*, *65*: 313-344.

[22] Zhao, C., 2021. Research on surface landing and moving guidance of small bodies with weak gravity. Master Thesis. Beijing Institute of Technology.

[23] Tiwari, M., Prazenica, R., & Henderson, T., 2023. Direct adaptive control of spacecraft near asteroids. *Acta Astronautica*, *202*: 197-213.

[24] Abe, S., Mukai, T., Hirata, N., Barnouin-Jha, O. S., Cheng, A. F., Demura, H., ... & Yoshikawa, M. 2006. Mass and local topography measurements of Itokawa by Hayabusa. *Science*, *312*(5778): 1344-1347.